

Dusty starburst galaxies in the early Universe as revealed by gravitational lensing

J. D. Vieira¹, D. P. Marrone², S. C. Chapman^{3,4}, C. De Breuck⁵, Y. D. Hezaveh⁶, A. Weiß⁷, J. E. Aguirre⁸, K. A. Aird⁹, M. Aravena⁵, M. L. N. Ashby¹⁰, M. Bayliss¹¹, B. A. Benson^{12,13}, A. D. Biggs⁵, L. E. Bleem^{12,14}, J. J. Bock^{1,15}, M. Bothwell², C. M. Bradford¹⁵, M. Brodwin¹⁶, J. E. Carlstrom^{12,13,14,17,18}, C. L. Chang^{12,13,18}, T. M. Crawford^{12,17}, A. T. Crites^{12,17}, T. de Haan⁶, M. A. Dobbs⁶, E. B. Fomalont²⁰, C. D. Fassnacht¹⁹, E. M. George²¹, M. D. Gladders^{12,17}, A. H. Gonzalez²², T. R. Greve²³, B. Gullberg⁵, N. W. Halverson²⁴, F. W. High^{12,17}, G. P. Holder⁶, W. L. Holzapfel²¹, S. Hoover^{12,13}, J. D. Hrubes⁹, T. R. Hunter²⁰, R. Keisler^{12,14}, A. T. Lee^{21,25}, E. M. Leitch^{12,17}, M. Lueker¹, D. Luong-Van⁹, M. Malkan²⁶, V. McIntyre²⁷, J. J. McMahon^{12,13,28}, J. Mehl^{12,17}, K. M. Menten⁷, S. S. Meyer^{12,13,14,17}, L. M. Mocanu^{12,17}, E. J. Murphy³¹, T. Natoli^{12,14}, S. Padin^{1,12,17}, T. Plagge^{12,17}, C. L. Reichardt²¹, A. Rest³², J. Ruel¹¹, J. E. Ruhl²⁹, K. Sharon^{12,17,30}, K. K. Schaffer^{12,33}, L. Shaw^{6,34}, E. Shirokoff¹, J. S. Spilker², B. Stalder¹⁰, Z. Staniszewski^{1,29}, A. A. Stark¹⁰, K. Story^{12,14}, K. Vanderlinde⁶, N. Welikala³⁵, R. Williamson^{12,17}

¹California Institute of Technology, 1200 E. California Blvd., Pasadena, CA 91125, USA

²Steward Observatory, University of Arizona, 933 North Cherry Avenue, Tucson, AZ 85721, USA

³Department of Physics and Atmospheric Science, Dalhousie University, Halifax, NS B3H 3J5 Canada

⁴Institute of Astronomy, University of Cambridge, Madingley Road, Cambridge CB3 0HA, UK

⁵European Southern Observatory, Karl-Schwarzschild Strasse, D-85748 Garching bei München, Germany

⁶Department of Physics, McGill University, 3600 Rue University, Montreal, Quebec H3A 2T8, Canada

⁷Max-Planck-Institut für Radioastronomie, Auf dem Hügel 69 D-53121 Bonn, Germany

⁸University of Pennsylvania, 209 South 33rd Street, Philadelphia, PA 19104, USA

⁹University of Chicago, 5640 South Ellis Avenue, Chicago, IL 60637, USA

¹⁰Harvard-Smithsonian Center for Astrophysics, 60 Garden Street, Cambridge, MA 02138, USA

¹¹Department of Physics, Harvard University, 17 Oxford Street, Cambridge, MA 02138, USA

¹²Kavli Institute for Cosmological Physics, University of Chicago, 5640 South Ellis Avenue, Chicago, IL 60637, USA

¹³Enrico Fermi Institute, University of Chicago, 5640 South Ellis Avenue, Chicago, IL 60637, USA

¹⁴Department of Physics, University of Chicago, 5640 South Ellis Avenue, Chicago, IL 60637, USA

USA

¹⁵Jet Propulsion Laboratory, 4800 Oak Grove Drive, Pasadena, CA 91109, USA

¹⁶Department of Physics and Astronomy, University of Missouri, 5110 Rockhill Road, Kansas City, MO 64110, USA

¹⁷Department of Astronomy and Astrophysics, University of Chicago, 5640 South Ellis Avenue, Chicago, IL 60637, USA

¹⁸Argonne National Laboratory, 9700 S. Cass Avenue, Argonne, IL, USA 60439, USA

¹⁹Department of Physics, University of California, One Shields Avenue, Davis, CA 95616, USA

²⁰National Radio Astronomy Observatory, 520 Edgemont Road, Charlottesville, VA 22903, USA

²¹Department of Physics, University of California, Berkeley, CA 94720, USA

²²Department of Astronomy, University of Florida, Gainesville, FL 32611, USA

²³Department of Physics and Astronomy, University College London, Gower Street, London WC1E 6BT, UK

²⁴Department of Astrophysical and Planetary Sciences and Department of Physics, University of Colorado, Boulder, CO 80309, USA

²⁵Physics Division, Lawrence Berkeley National Laboratory, Berkeley, CA 94720, USA

²⁶Department of Physics and Astronomy, University of California, Los Angeles, CA 90095-1547, USA

²⁷Australia Telescope National Facility, CSIRO, Epping, NSW 1710, Australia

²⁸Department of Physics, University of Michigan, 450 Church Street, Ann Arbor, MI, 48109, USA

²⁹Physics Department, Center for Education and Research in Cosmology and Astrophysics, Case Western Reserve University, Cleveland, OH 44106, USA

³⁰Department of Astronomy, University of Michigan, 500 Church Street, Ann Arbor, MI, 48109, USA

³¹Observatories of the Carnegie Institution for Science, 813 Santa Barbara Street, Pasadena, CA 91101, USA

³²Space Telescope Science Institute, 3700 San Martin Dr., Baltimore, MD 21218, USA

³³Liberal Arts Department, School of the Art Institute of Chicago, 112 S Michigan Ave, Chicago, IL 60603, USA

³⁴Department of Physics, Yale University, P.O. Box 208210, New Haven, CT 06520-8120, USA

³⁵Institut d'Astrophysique Spatiale, Bâtiment 121, Université Paris-Sud XI & CNRS, 91405 Orsay Cedex, France

In the past decade, our understanding of galaxy evolution has been revolutionized by the discovery that luminous, dusty, starburst galaxies were 1,000 times more abundant in the early Universe than at present^{1,2}. It has, however, been difficult to measure the complete redshift

distribution of these objects, especially at the highest redshifts ($z > 4$). Here we report a redshift survey at a wavelength of three millimeters, targeting carbon monoxide line emission from the star-forming molecular gas in the direction of extraordinarily bright millimetre-wave-selected sources. High-resolution imaging demonstrates that these sources are strongly gravitationally lensed by foreground galaxies. We detect spectral lines in 23 out of 26 sources and multiple lines in 12 of those 23 sources, from which we obtain robust, unambiguous redshifts. At least 10 of the sources are found to lie at $z > 4$, indicating that the fraction of dusty starburst galaxies at high redshifts is greater than previously thought. Models of lens geometries in the sample indicate that the background objects are ultra-luminous infrared galaxies, powered by extreme bursts of star formation.

We constructed a catalog of high-redshift ($z > 1$) galaxy candidates from the first 1,300 square degrees of the South Pole Telescope (SPT)³ survey by selecting sources with dust-like spectral indexes in the 1.4 and 2.0 mm SPT bands⁴. A remarkable aspect of selecting sources based on their flux at millimetre wavelengths is the so-called “negative k -correction”⁵, whereby cosmological dimming is compensated by the steeply rising dust spectrum as the source redshift increases. As a result, a millimetre-selected sample should draw from the redshift distribution of dusty starburst galaxies with little bias over the entire redshift range in which they are expected to exist. To isolate the high-redshift, dusty-spectrum galaxy population, sources with counterparts in the IRAS Faint Source Catalog⁶ (typically $z < 0.03$) were removed, and those with counterparts in the 843 MHz Sydney University Molonglo Sky Survey⁷ were removed to exclude sources with strong synchrotron emission (e.g. flat-spectrum radio quasars) that may have passed the spectral index cut. A sample of 47 sources with 1.4 mm flux density > 20 mJy and accurate positions were selected for high-resolution imaging with the Atacama Large Millimeter/sub-millimeter Array (ALMA). The ALMA spectroscopic observations targeted a sample of 26 sources, all but two of which are in the imaging sample (see Supplementary Information). These objects are among the brightest dusty-spectrum sources in the $z > 0.1$ extragalactic sky at millimetre wavelengths.

Gravitationally lensed sources are expected to predominate in samples of the very brightest dusty galaxies because of the rarity of unlensed dusty, starburst galaxies at these flux levels^{8–10}. Massive elliptical galaxies, acting as lenses, will have Einstein radii as large as $2''$ and may magnify background galaxies by factors of 10 or more. To confirm the lensing hypothesis and determine magnifications, we imaged 47 SPT sources with ALMA at $870 \mu\text{m}$ in two array configurations, which provide angular resolutions of $1.5''$ and $0.5''$ (FWHM). A sample of these objects with IR imaging, spectroscopic redshifts, and resolved structure is shown in Figure 1. Integration times of only one minute per source are adequate to show that the sources are resolved into arcs or Einstein

rings – hallmarks of gravitational lensing – in most sources. For all sources for which we have IR and submillimetre imaging, as well as spectroscopic redshifts, the emission detected by ALMA coincides with massive foreground galaxies or galaxy groups/clusters, but is spatially distinct and at drastically different redshifts (see Figures 2 and S.3). Using a modeling procedure that treats the interferometer data in their native measurement space, rather than through reconstructed sky images, to simultaneously determine the source/lens configuration and correct for antenna-based phase errors¹¹, we are able to determine magnifications and derive intrinsic luminosities for our sources. Complete models of four lenses¹¹, as well as preliminary models of eight more, indicate lensing magnifications between 4 and 22. After correcting for the magnification, these sources are extremely luminous – more than $10^{12}L_{\odot}$ and sometimes $> 10^{13}L_{\odot}$ – implying star formation rates in excess of $500 M_{\odot}\text{yr}^{-1}$.

Obtaining spectroscopic redshifts for high-redshift, dusty starburst galaxies has been notoriously difficult. To date, most spectroscopic redshift measurements have come from the rest-frame ultraviolet and optical wavebands after multi-wavelength counterpart identification^{2,12,13}. These observations are difficult owing to the extinction of the UV light by the dust itself, the cosmological dimming, and the ambiguity in the association of the dust emission with multiple sources of optical emission visible in deep observations. A much more direct method to determine redshifts of starburst galaxies, particularly at high redshift, is through observations of molecular emission associated with their dusty star forming regions. The millimetre and submillimetre transitions of molecular carbon monoxide (CO) and neutral carbon (C I) are well-suited for this purpose¹⁴. These emission lines are a major source of cooling for the warm molecular gas fueling the star formation, and can thus be related unambiguously to the submillimetre continuum source¹⁵. Until recently, bandwidth and sensitivity limitations made this approach time-intensive. The combination of ALMA – even with its restricted early science capabilities and only 16 antennas – and a unique sample of extraordinarily bright millimetre sources has changed this situation dramatically, allowing us to undertake a sensitive, systematic search for molecular and atomic lines across broad swaths of redshift space at $z > 1$.

We conducted a redshift search in the 3 mm atmospheric transmission window with ALMA using five spectral tunings of the ALMA receivers to cover 84.2 – 114.9 GHz. For $z > 1$ at least one CO line will fall in this frequency range, except for a small redshift “desert” ($1.74 < z < 2.00$). For sources at $z > 3$, multiple transitions (such as $\text{CO}(J_{\text{up}} > 3)$ and $\text{C I}(^3P_1 \rightarrow ^3P_0)$) are redshifted into the observing band, allowing for an unambiguous redshift determination. We find one or more spectral features in 23 of 26 SPT-selected sources. The detections comprise

44 emission line features which we identify as redshifted emission from molecular transitions of ^{12}CO , ^{13}CO , H_2O and H_2O^+ , and a C I fine structure line. The spectra of all sources are shown in Figure 2. For 18 of the sources we are able to infer unique redshift solutions, either from ALMA data alone (12), or with the addition of data from the Very Large Telescope and/or the Atacama Pathfinder Experiment telescope (6). With the 10 $z > 4$ objects discovered here, we have more than doubled the number of spectroscopically confirmed, ultra-luminous galaxies discovered at $z > 4$ in millimetre/submillimetre surveys in the literature (of which just nine have been reported previously^{13,14,16-21}). Two sources are at $z = 5.7$, placing them among the most distant ultra-luminous starburst galaxies known.

The SPT dusty galaxy redshift sample comprises 28 sources, as we include an additional two SPT sources with spectroscopic redshifts²² that would have been included in the ALMA program had their redshifts not already been determined. Of the 26 ALMA targets, three lack a spectral line feature in the ALMA band. We tentatively and conservatively place these at $z = 1.85$, in the middle of the $z = 1.74 - 2.00$ redshift desert, though it is also possible that they are located at very high redshift or have anomalously faint CO lines. For the five sources for which only a single emission line is found, only two or three redshifts are possible (corresponding to two choices of CO transition) after excluding redshift choices for which the implied dust temperature, derived from our extensive millimetre/submillimetre photometric coverage (provided by ALMA 3 mm, SPT 2 & 1 mm, APEX/LABOCA 870 μm and *Herschel*/SPIRE 500, 350, 250 μm observations²³), is inconsistent with the range seen in other luminous galaxies²². For these sources we adopt the redshift corresponding to the dust temperature closest to the median dust temperature in the unambiguous spectroscopic sample, as shown in Figure 2.

The cumulative distribution function of all redshifts in this sample is shown in Figure 3. The median redshift of our full sample is $z_{\text{med}} = 3.5$. The redshift distribution of SPT sources with mm spectroscopic redshifts is in sharp contrast to that of radio-identified starbursts with optical spectroscopic redshifts, which have a significantly lower median redshift of $z_{\text{med}} = 2.2$, and for which only 15-20% of the population is expected to be at $z > 3$ ². Part of this difference can be attributed to the high flux threshold of the original SPT selection, which effectively requires that the sources be gravitationally lensed. A much smaller total volume is lensed at $z < 1$ than at higher redshift, and, as expected, we do not find any such sources in the SPT sample²³. However, if we only compare sources at $z > 2$ (the lowest confirmed spectroscopic redshift in the SPT sample), the median redshift of the radio-identified sample is still significantly lower (2.6) than the SPT sample, and the probability that both samples are drawn from the same distribution is

$< 10^{-5}$ by the Kolmogorov-Smirnov test. A recently published survey²⁴ of millimetre-identified starbursts with optical counterparts determined from high resolution mm imaging and redshifts measured from optical spectroscopy or estimated from optical photometry found a median redshift of $z_{\text{med}} = 2.8$. Again comparing the distribution of sources at $z > 2$, the probability that these objects and the SPT-selected sources are drawn from the same parent distribution is 0.43, indicating rough consistency between our secure redshift determinations and the distribution estimated from the optical methods. A full analysis of the molecular line detections, redshift determinations, residual selection effects, and a derivation of the intrinsic redshift distribution for the SPT sample is reported in a companion paper²³.

These 26 sources represent less than 25% of the recently completed SPT survey and catalog. This newly discovered population of high-redshift starbursts will enrich our understanding of obscured star formation in the early universe. Existing semi-analytic hierarchical models of galaxy evolution^{25,26} have already had difficulties reconciling the number of $z \approx 4$ systems inferred from previous observational studies^{13,24}. The presence of two intensely starbursting galaxies at $z = 5.7$, 1 Gyr after the Big Bang, in a sample of just 26 sources, demonstrates that significant reservoirs of dust and molecular gas had been assembled by the end of the epoch of cosmic reionization. As the millimetre-brightest high-redshift starbursts in the sky, the present sample will be key targets for ALMA studies of star formation physics at high redshift. The gravitational lensing of these sources provides access to diagnostic information from molecular lines that would otherwise take hundreds of times longer to observe, and effective source-plane resolution several times higher than can otherwise be achieved.

1. Lagache, G., Puget, J.-L. & Dole, H. Dusty Infrared Galaxies: Sources of the Cosmic Infrared Background. *Ann. Rev. Astron. Astrophys.* **43**, 727–768 (2005). arXiv:astro-ph/0507298.
2. Chapman, S. C., Blain, A. W., Smail, I. & Ivison, R. J. A Redshift Survey of the Submillimeter Galaxy Population. *Astrophys. J.* **622**, 772–796 (2005). arXiv:astro-ph/0412573.
3. Carlstrom, J. E. *et al.* The 10 Meter South Pole Telescope. *Pub. Astron. Soc. Pac.* **123**, 568–581 (2011).
4. Vieira, J. D. *et al.* Extragalactic Millimeter-wave Sources in South Pole Telescope Survey Data: Source Counts, Catalog, and Statistics for an 87 Square-degree Field. *Astrophys. J.* **719**, 763–783 (2010). 0912.2338.
5. Blain, A. W. & Longair, M. S. Submillimetre Cosmology. *Mon. Not. R. Astron. Soc.* **264**, 509–521 (1993).
6. Moshir, M., Kopman, G. & Conrow, T. A. O. (eds.) *IRAS Faint Source Survey, Explanatory supplement version 2* (Pasadena: Infrared Processing and Analysis Center, California Institute of Technology, 1992, edited by Moshir, M.; Kopman, G.; Conrow, T. a.o., 1992).
7. Bock, D. C.-J., Turtle, A. J. & Green, A. J. A High-Resolution Radio Survey of the VELA Supernova Remnant. *Astron. J.* **116**, 1886–1896 (1998). arXiv:astro-ph/9807125.
8. Blain, A. W. Galaxy-galaxy gravitational lensing in the millimetre/submillimetre waveband. *Mon. Not. R. Astron. Soc.* **283**, 1340–1348 (1996).
9. Negrello, M. *et al.* Astrophysical and cosmological information from large-scale submillimetre surveys of extragalactic sources. *Mon. Not. R. Astron. Soc.* **377**, 1557–1568 (2007). arXiv:astro-ph/0703210.
10. Hezaveh, Y. D. & Holder, G. P. Effects of Strong Gravitational Lensing on Millimeter-wave Galaxy Number Counts. *Astrophys. J.* **734**, 52–59 (2011). 1010.0998.
11. Hezaveh, Y. D. *et al.* ALMA Observations of Strongly Lensed Submillimeter Galaxies. *submitted to ApJ* (2012).
12. Ivison, R. J. *et al.* Deep radio imaging of the SCUBA 8-mJy survey fields: submillimetre source identifications and redshift distribution. *Mon. Not. R. Astron. Soc.* **337**, 1–25 (2002). arXiv:astro-ph/0206432.

13. Coppin, K. E. K. *et al.* A submillimetre galaxy at $z = 4.76$ in the LABOCA survey of the Extended Chandra Deep Field-South. *Mon. Not. R. Astron. Soc.* **395**, 1905–1914 (2009). 0902.4464.
14. Walter, F. *et al.* The intense starburst HDF 850.1 in a galaxy overdensity at $z \approx 5.2$ in the Hubble Deep Field. *Nature* **486**, 233–236 (2012). 1206.2641.
15. Solomon, P. M. & Vanden Bout, P. A. Molecular Gas at High Redshift. *Ann. Rev. Astron. Astrophys.* **43**, 677–725 (2005). arXiv:astro-ph/0508481.
16. Capak, P. *et al.* Spectroscopic Confirmation of an Extreme Starburst at Redshift 4.547. *Astrophys. J. Lett.* **681**, L53–L56 (2008). 0806.0657.
17. Daddi, E. *et al.* Two Bright Submillimeter Galaxies in a $z = 4.05$ Protocluster in Goods-North, and Accurate Radio-Infrared Photometric Redshifts. *Astrophys. J.* **694**, 1517–1538 (2009). 0810.3108.
18. Daddi, E. *et al.* A CO Emission Line from the Optical and Near-IR Undetected Submillimeter Galaxy GN10. *Astrophys. J. Lett.* **695**, L176–L180 (2009). 0903.3046.
19. Riechers, D. A. *et al.* A Massive Molecular Gas Reservoir in the $z = 5.3$ Submillimeter Galaxy AzTEC-3. *Astrophys. J. Lett.* **720**, L131–L136 (2010). 1008.0389.
20. Cox, P. *et al.* Gas and Dust in a Submillimeter Galaxy at $z = 4.24$ from the Herschel Atlas. *Astrophys. J.* **740**, 63–72 (2011). 1107.2924.
21. Combes, F. *et al.* A bright $z = 5.2$ lensed submillimeter galaxy in the field of Abell 773. HLSJ091828.6+514223. *Astron. Astrophys.* **538**, L4–L7 (2012). 1201.2908.
22. Greve, T. R. *et al.* Submillimeter Observations of Millimeter Bright Galaxies Discovered by the South Pole Telescope. *Astrophys. J.* **756**, 101–113 (2012). 1206.4550.
23. Weiß, A. *et al.* ALMA redshifts of millimeter selected galaxies from the SPT survey. *Astrophys. J.* (2012). Submitted.
24. Smolcic, V. *et al.* Millimeter imaging of submillimeter galaxies in the COSMOS field: Redshift distribution. *ArXiv e-prints* (2012). 1205.6470.
25. Baugh, C. M. *et al.* Can the faint submillimetre galaxies be explained in the Λ cold dark matter model? *Mon. Not. R. Astron. Soc.* **356**, 1191–1200 (2005). arXiv:astro-ph/0406069.

26. Benson, A. J. GALACTICUS: A semi-analytic model of galaxy formation. *New Astron.* **17**, 175–197 (2012). 1008.1786.
27. Banerji, M. *et al.* Luminous starbursts in the redshift desert at $z \sim 1 - 2$: star formation rates, masses and evidence for outflows. *Mon. Not. R. Astron. Soc.* **418**, 1071–1088 (2011). 1108.0420.
28. Egami, E. *et al.* APM 08279+5255: Keck Near- and Mid-Infrared High-Resolution Imaging. *Astrophys. J.* **535**, 561–574 (2000). arXiv:astro-ph/0001200.

Acknowledgements The SPT is supported by the National Science Foundation, the Kavli Foundation and the Gordon and Betty Moore Foundation. ALMA is a partnership of ESO (representing its member states), NSF (USA) and NINS (Japan), together with NRC (Canada) and NSC and ASIAA (Taiwan), in cooperation with the Republic of Chile. The Joint ALMA Observatory is operated by ESO, AUI/NRAO and NAOJ. The National Radio Astronomy Observatory is a facility of the National Science Foundation operated under cooperative agreement by Associated Universities, Inc. Partial support for this work was provided by NASA from the Space Telescope Science Institute. This work is based in part on observations made with *Herschel*, a European Space Agency Cornerstone Mission with significant participation by NASA. Work at McGill is supported by NSERC, the CRC program, and Cifar.

Author Contributions JDV and DPM wrote the text. SCC took and reduced optical images and spectroscopy. AW, CDB, and DPM analyzed the ALMA spectra. DPM, JSS and YH analyzed the ALMA imaging data. JDV reduced and analysed the *Herschel* data. YH constructed the lens models. CDF reduced optical images. All other authors (listed alphabetically) have contributed as part of the South Pole Telescope collaboration, by either their involvement with the construction of the instrument, the initial discovery of the sources, or multi-wavelength follow-up, and/or contributions to the text.

Competing Interests The authors declare that they have no competing financial interests.

Correspondence Correspondence and requests for materials should be addressed to J.D.V. (email: vieira@caltech.edu).

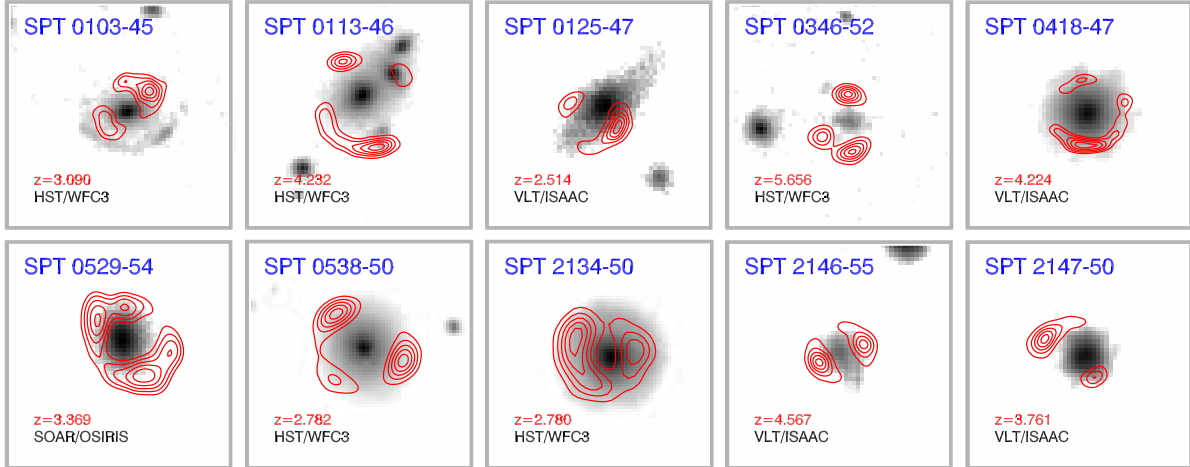
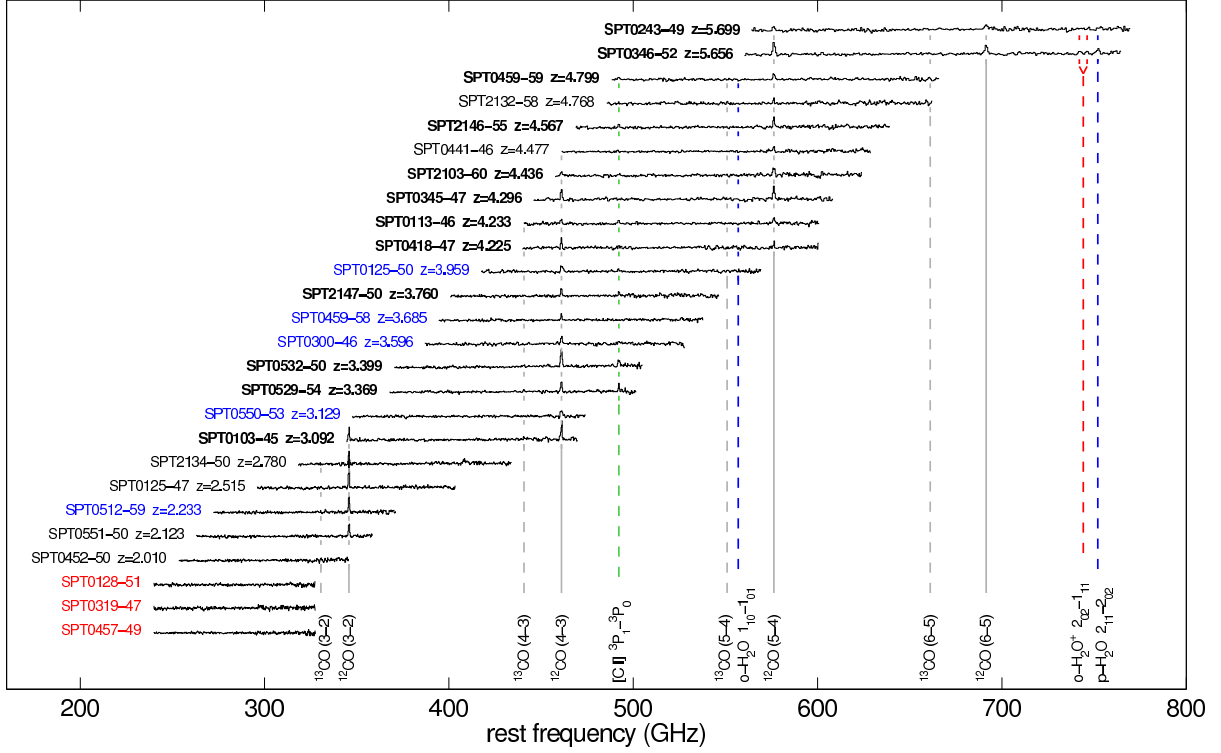


Figure 1: **Figure 1:** Near-infrared (NIR) and ALMA submillimeter-wavelength images of SPT targets. Images are $8'' \times 8''$. We show 10 sources for which we have confirmed ALMA spectroscopic redshifts, deep NIR imaging, and well-resolved structure in the ALMA $870 \mu\text{m}$ imaging. The greyscale images are NIR exposures from the *Hubble Space Telescope* (co-added F160W and F110W filters), the Very Large Telescope (K_s), or the Southern Astrophysical Research Telescope (K_s), and trace the starlight from the foreground lensing galaxy. The NIR images are shown with logarithmic stretch. The red contours are ALMA $870 \mu\text{m}$ imaging showing the background source structure, clearly indicative of strong lensing from galaxy-scale halos. In all cases, the contours start at 5σ and are equally spaced up to 90% of the peak significance, which ranges from 12 to 35. Spectroscopic redshifts of the background sources are shown in red in each panel. The ALMA exposures were approximately 2-minute integrations, roughly equally divided between the compact and extended array configurations. The resulting resolution is $0.5''$. SPT 0103–45 shows a rare lensing configuration of one lens and two background sources at different redshifts, one visible with ALMA and one with HST. SPT 0346–52, with a CO-derived redshift of $z=5.656$, is among the highest-redshift starbursts known. (See the Supplementary Information for more details.)



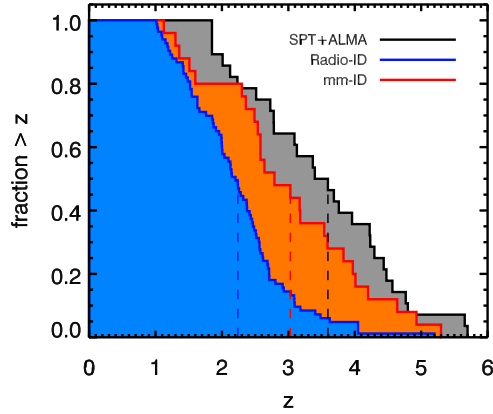


Figure 3: **Figure 3:** The cumulative redshift distribution of luminous, dusty starburst galaxies, as measured with different techniques. The SPT millimetre-selected sample, with redshifts directly determined from spectroscopic observations of the molecular gas in the galaxies, is shown in black. The existing samples of radio-identified starbursts^{2, 14, 17, 18, 27} with redshifts determined from rest-frame ultraviolet spectroscopy, are compiled in the blue distribution. The redshift distribution²⁴ of millimetre-identified starburst galaxies in the COSMOS survey is shown in red/orange, though the majority of redshifts in this sample are derived from optical/IR photometry of the sources rather than spectroscopy, and therefore less certain. Sources at $z < 1$ were removed from the previous samples of starburst galaxies to better compare to the selection effect imposed on the SPT sample due to gravitational lensing. The distribution of redshifts for radio-identified sources is incompatible with the distribution for the sample presented in this work. This measurement demonstrates that the fraction of dusty starburst galaxies at high-redshift is greater than previously derived and that radio-identified samples were biased to lower redshift than the underlying population.

Sample Selection

The dusty-spectrum sources targeted for the ALMA observations described here were found in the SPT survey. The full survey comprises 2540 deg² of mapped sky, but constraints of data analysis and followup limited the area available for target selection at the time of the ALMA Cycle 0 deadline to 1300 deg². The initial SPT target list was extracted from the SPT maps according to the procedure described in a previous paper⁴ and the selection outlined in the manuscript. Before observing these sources with ALMA, we required that they have followup observations with the LABOCA 870 μm camera on the Atacama Pathfinder Experiment telescope to improve the accuracy of their positions. At the time of the ALMA Cycle 0 proposal deadline, we had completed this followup for 76 sources within 1300 deg² of the survey area. We selected 47 sources for imaging and 26 sources for spectroscopy with ALMA; 24 of the 26 spectroscopic sources were also in the imaging sample. The sample selection targeted sources with the highest SPT 1.4 mm fluxes, subject to the restrictions of the ALMA call for proposals. The most important restriction was the requirement that sources be located within 15 degrees of each other on the sky. This should not affect the statistical properties of the sample, however, it merely prevented the observation of a complete set of SPT sources above a defined flux threshold.

Detected line features

The detected CO and C₁ line features are shown in Figure S.4. Additional lines are detected in some spectra, including ¹³CO transitions in two sources. However, the detection of both ¹²CO and ¹³CO transitions in the same source does not break redshift degeneracies because both transitions are harmonically spaced; at a given frequency of detection, every pair of CO isotopic transitions of the same rotational level (J) will have the same observed spacing. Emission lines of H₂O and H₂O⁺ are detected in the spectrum of SPT0346-52.

ALMA imaging

Continuum images from the ALMA observations at both wavelengths are shown in Figure S.5 for all 49 sources observed with ALMA in one or both of the 3 mm redshift search or the 870 μm imaging projects. The positional coincidence between the bands confirms that the redshifts are derived for the same objects that are seen to show structures indicative of gravitational lensing. Nearly all sources are resolved at the 0.5'' resolution of the 870 μm data, most likely due to gravitational lensing. Exceptions may be due to lensing by groups/clusters, with image counterparts that are either faint or too widely separated to be detected in the small (18'') primary beam of the ALMA antennas at this wavelength, or because some of our objects have small image separations. Lensed dusty sources with similar image separations are already prominent in the literature, in-

cluding APM 08279+5255²⁸, which has three images separated by $<0.4''$. Conclusive evidence of lensing in many objects, including the most compact, awaits IR imaging and spectroscopic redshifts for the sources (and any candidate lens galaxies). The 23 objects for which we have the most complete data (the 26 sources of the 3 mm spectroscopic sample, less three without detected lines, less two without IR imaging, augmented by the two sources²² for which we had prior redshifts) are shown in Figure S.6.

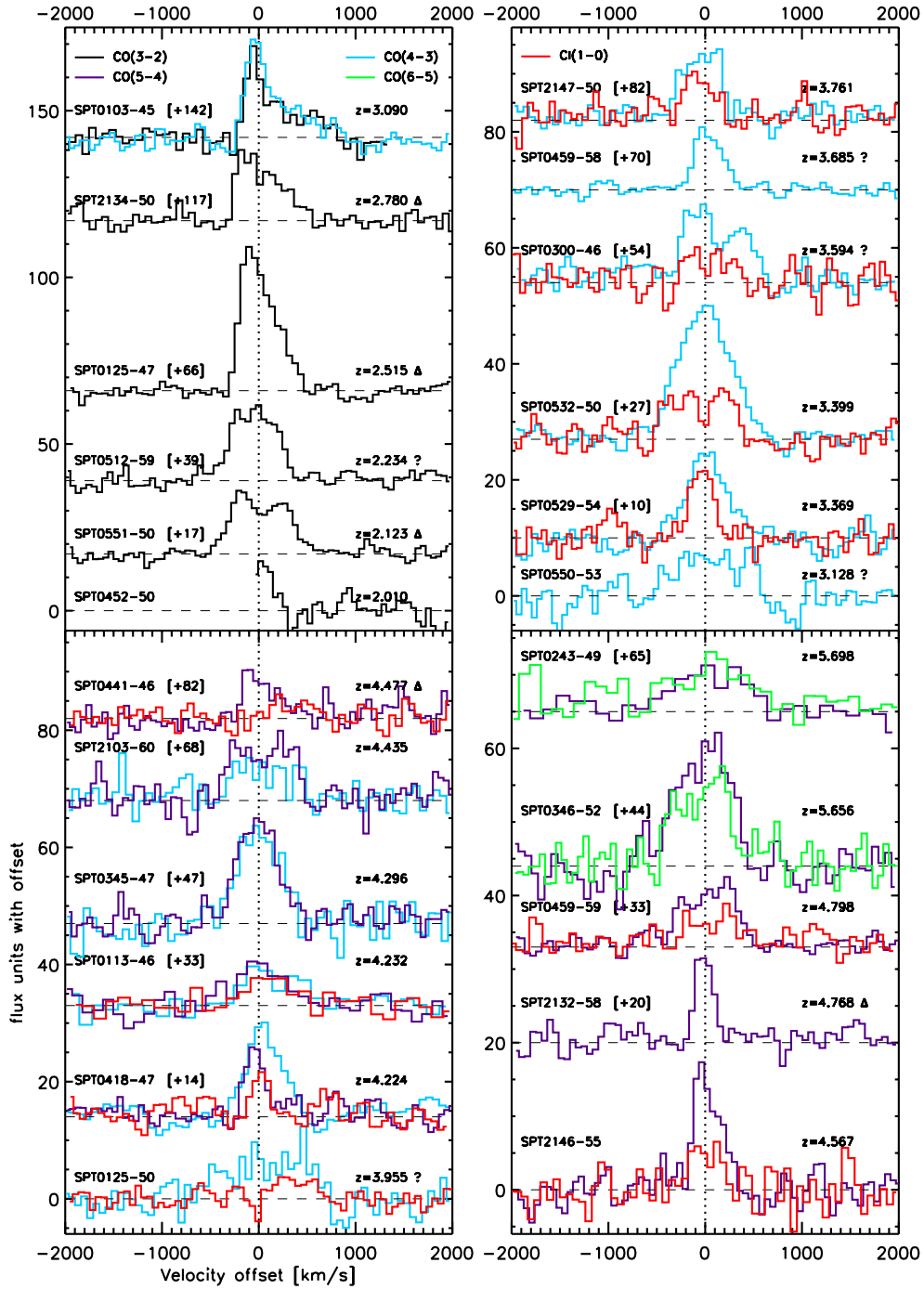


Figure S.4: The CO(3-2), CO(4-3), CO(5-6), CO(6-5) and C_I(1-0) emission lines observed with ALMA for 23 out of the 26 SPT sources, which were used to determine the source redshifts. The vertical axis is observed flux density, sources are offset from zero for clarity with the offsets specified in square brackets next to the source names. Redshifts marked with ‘Δ’ are confirmed using additional observations from other facilities²³, while redshifts marked with ‘?’ are uncertain and are shown at the most likely redshift. SPT0452-50 has a single line, but is determined to be at $z = 2.010$ rather than $z = 1.007$ because the implied dust temperature for this source would be far lower than in any other source (13 K) were it at the lower redshift²³.

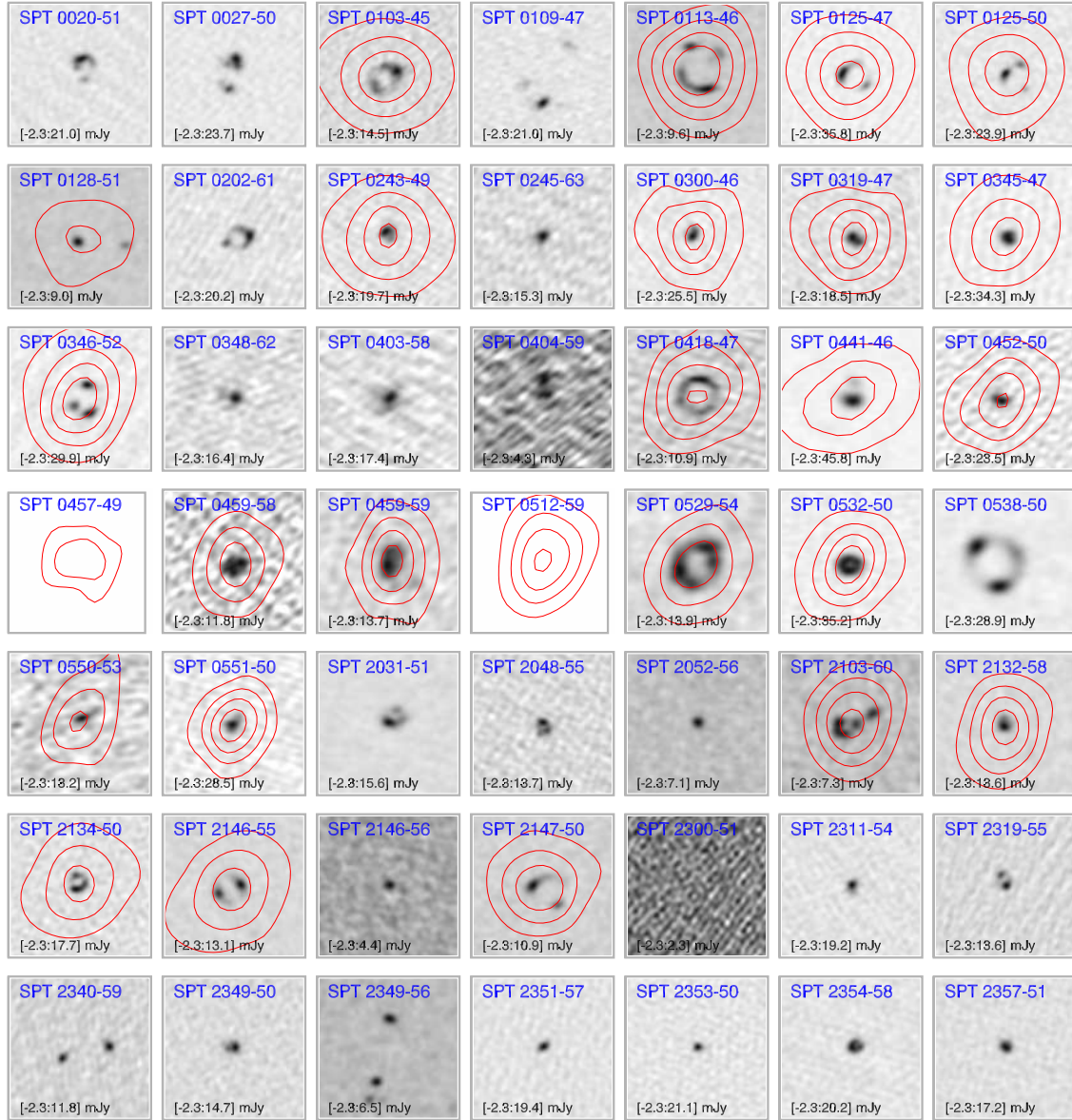


Figure S.5: Continuum images of the 49 sources observed at 3 mm and/or 870 μm wavelength with ALMA. The 47 sources for which 870 μm data were acquired are shown in greyscale, with the 3 mm images overlaid in red contours. Two sources from the redshift sample that lack 870 μm data appear as red contours on a blank background. Images are $10'' \times 10''$, the 870 μm and 3 mm images have $0.5''$ and $5''$ resolution, respectively. The correspondence between the positions at the two wavelengths unambiguously links the lensing structure visible at 870 μm to the 3 mm spectra. The 3 mm contours are plotted in units of 3σ , starting at 3σ for sources at $S/N < 15$, and 5σ for sources at $S/N > 15$, except SPT 0457-49, where the contours are 3 and 4σ . The grey scale stretch of each image is indicated in the lower left hand side of each panel and is roughly from -1σ to the peak value.

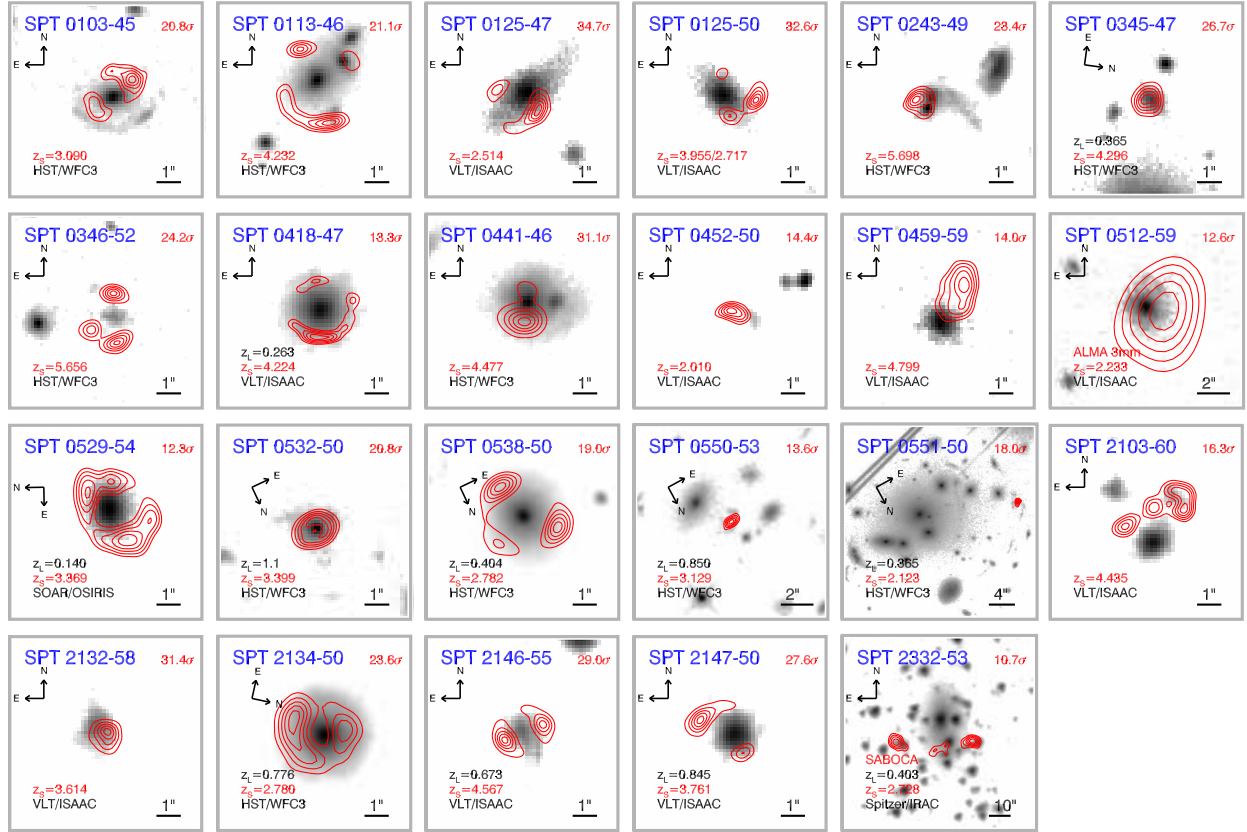


Figure S.6: Images of the full set of 23 sources for which we have ALMA 870 μm 3 mm, or SABOCA 350 μm imaging, deep NIR imaging, and a redshift for the background galaxy (including ambiguous redshifts). Except for SPT 0512-59, ALMA 870 μm emission is represented with 5 red contours, spaced linearly from five times the image noise to 90% of the peak signal to noise, specified in the upper right of each panel. For SPT 0512-59, which lacks ALMA 870 μm data, we show the ALMA 3 mm continuum contours. For SPT 2332-53, which lacks ALMA 870 μm data, we show the APEX/SABOCA 350 μm continuum contours. The redshift of the background source (z_s) is specified in red. Greyscale images are near-infrared exposures from the *Hubble Space Telescope* (co-added F160W and F110W filters), the Very Large Telescope (K_s), the Southern Astrophysical Research Telescope (K_s), or the *Spitzer Space Telescope* (3.6 μm) and trace the starlight from the foreground lensing galaxy. The images are shown with logarithmic stretch. When known, the redshift of the foreground galaxy (z_L) is specified in black. In nearly every case, there is a coincidence of the millimetre/submillimetre emission, determined by the redshift search data to arise at high redshift, with a lower redshift galaxy, a galaxy group, or a cluster. This is precisely the expectation for gravitationally lensed galaxies. Three cluster lenses are apparent, SPT 0550-53, SPT 0551-50, and SPT 2332-53, with two other systems lensed by compact groups (SPT 0113-46, SPT 2103-60).